Scale Effects in Cellular Metals

Onck, P.R.

Published in:
MRS Bulletin

Scale Effects in Cellular Metals

P.R. Onck

Abstract

Scale effects in cellular metals can develop when the specimen size is of the order of the cell size. Decreasing the relevant specimen dimensions—height, width, and ligament size (the region between notches in notched specimens)—leads to material strengthening in shear, in indentation, and in notched specimens and to reduced strength and stiffness in uniaxial compression. Experimental size-effect studies were reviewed, and it was concluded from discrete modeling results that scale effects are caused by two different microstructural mechanisms: boundary-layer effects and constraint effects. The first mechanism is active in shear (strong boundary layers) and uniaxial compression (weak boundary layers) and vanishes for specimens larger than two cell sizes and seven cell sizes, respectively. The second mechanism is active in indentation and in notched specimens, leading to a strengthening behavior that is inversely proportional to indenter and ligament size.

Keywords: *cellular metals, mechanical properties, size effects.*

Introduction

Cellular metals are emerging as a new class of engineering materials with high potential in sandwich structures, energy absorption, and heat dissipation.[1,2] They inherit their attractive thermomechanical properties directly from their cellular microstructure. Most commercial metallic foams have cell sizes ranging roughly from 1 mm to 10 mm. Reduction of the cell size to <1 mm is often restricted due to manufacturing constraints. This means that in many applications, the components can have dimensions of only a few cell sizes. Consequently, the cell size becomes an essential length scale in the problem, making the mechanical behavior of cellular solids scale-dependent.

An important manifestation of scale dependency is the occurrence of size effects in the mechanical testing of metallic foams. The term "size effect" designates the influence of the specimen size, relative to the cell size, on mechanical properties like stiffness and strength. Recent experimental studies[3,4] have shown that under uniaxial compression, stiffness and strength decrease with decreasing specimen size. Alternatively, in the case of simple shear[3,5] and indentation,[3,6] strength increases with decreasing specimen/indenter size, as explained in the discussion section of this article.

Another manifestation of scale dependency is the effect of notches and cracks on the strength of metallic foams. Experiments on specimens of fixed width with two side notches, called double-edge-notched (DEN) specimens, show increasing material strength between the notches when the notch size is increased.[7–12] However, specimens with cracks in the center of the specimen do not show this effect.[13] In this article, some of the experimental results are reviewed, accompanied by modeling results to trace the microstructural origin of the different scale effects.

Size Effects

In this section, experimental as well as modeling results are discussed with respect to size effects under uniaxial compression, simple shear, and indentation. For details about the experimental procedures, see Reference 3; here, only the essentials are reiterated. For the mechanical testing, a nominally 7% dense open-cell aluminum (6101-T6) foam (trade name Duocel) and a nominally 8% dense closed-cell aluminum foam (trade name Alporas) were used.

Uniaxial Compression

Uniaxial-compression tests were performed on cylinders of the open-cell foam (Duocel) with a height-to-diameter ratio of 2. For the closed-cell foam (Alporas), square prisms with a height-to-width ratio of 2 were used. The specimen geometry was kept fixed, while the absolute dimensions were varied. To avoid the effects of early localized plasticity, the unloading modulus was measured for greater accuracy. Figure 1a shows the unloading modulus E^* normalized by the bulk value E^*_{bulk} valid for very large specimens (E^*_{bulk} = 943 MPa for Alporas and E^*_{bulk} = 368 MPa for Duocel). The normalized Young's modulus was plotted against specimen size L normalized by the cell size d (d = 3 mm for Duocel and d = 4.5 mm for Alporas). Each

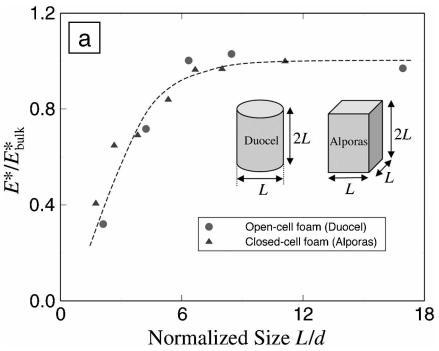

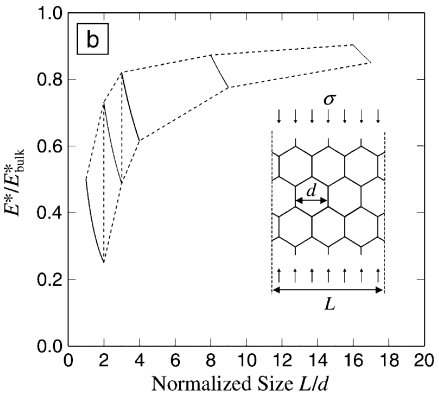

Figure 1. (a) Experimental unloading modulus E* *normalized by the bulk value* E^*_{bulk}*, plotted against specimen size* L *normalized by the cell size* d*, for specimens of open-cell (Duocel) and closed-cell (Alporas) foam. Each data point represents the average of 5–9 specimens for Alporas and 3–5 specimens for Duocel. The Young's modulus* E* *decreases with decreasing specimen size, and the bulk value is attained for specimens with* L *of at least seven cell diameters. (b) Theoretical Young's modulus* E* *of an infinitely long hexagonal honeycomb (see inset) of finite width* L *normalized by the bulk value for infinite width* E^*_{bulk}*, plotted against* L/d*. Stiffness values drop for smaller specimens and converge to the bulk stiffness for large specimens.*

data point in Figure 1a represents the average of 5–9 specimens for Alporas and 3–5 specimens for Duocel. Figure 1a clearly indicates that the Young's modulus E^* decreases with decreasing specimen size, and the bulk value is attained for specimens with a size L of at least seven cell diameters.

Similar results were obtained for the plastic collapse strength.[3] The regular hexagonal structure was adopted as a two-dimensional (2D) model material because cell-wall bending is its major deformation mechanism, similar to real three-dimensional (3D) foams. An infinitely long, regular hexagonal honeycomb was considered, as shown in the inset of Figure 1b. The cell walls were assumed to be elastic and were treated as Euler–Bernoulli beams of length l and thickness t with Young's modulus E_s, where the subscript refers to the solid material from which the cellular material is made.[14] Figure 1b shows the results for the Young's modulus E^* normalized by the value for an infinitely wide honeycomb:[15]

$$E^*_{\text{bulk}} = 4/\sqrt{3}E_s(t/l)^3. \quad (1)$$

The stiffness is discontinuous at integer values of L/d because each integer value adds another load-carrying beam. In our analysis, the number of load-carrying vertical beams increases discretely with L/d. In a random structure (e.g., a foam), this will clearly not be the case. To account for this in an average manner, a scatter band was constructed by connecting the maxima as well as the minima of the L/d intervals (Figure 1b). Clearly, the stiffness drops for smaller specimens and converges to the bulk stiffness for large specimens. The origin of this trend can be traced back to two contributions: the decreased constraint at the free surface, making the surface cells more compliant; and the area fraction of cut cell walls at the boundary, which remain stress-free. Similar results were obtained for the plastic collapse strength using limit-load analysis.[14]

Shear

The shear strength of the closed-cell foam (Alporas) was measured according to ASTM Standard C 273, with the specimen adhesively bonded to rigid plates (see inset of Figure 2a). Five different thicknesses were tested for a fixed length/thickness ratio of 12. The out-of-plane width was chosen to be 50 mm. Figure 2 shows the peak strength τ^*_{peak} normalized by the bulk value, $\tau^*_{\text{bulk}} = 1.02$ MPa, as a function of normalized thickness T/d ($d = 4.5$ mm). For the four thickest specimens, each data point is the average of three tests, while

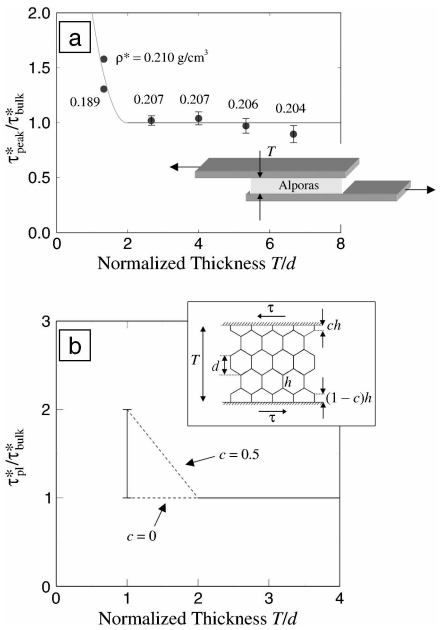

Figure 2. (a) Experimental shear strength τ^*_{peak} normalized by the bulk value τ^*_{bulk}, plotted against specimen thickness T *normalized by the cell size* d, *of a specimen adhesively bonded to rigid plates (see inset). ρ^* is the density of the foam. (b) Theoretical shear strength τ^*_{pl} normalized by the bulk value τ^*_{bulk}, plotted against specimen thickness* T *normalized by the cell size* d, *for a regular hexagonal honeycomb (see inset). The length of a cell wall is given by* h; c *is a multiplier between 0 and 1 that accounts for the varying lengths of partial cell walls at the boundaries.*

for the smallest thickness, the individual data points are plotted. Next to each data point, the density is indicated. Contrary to the uniaxial-compression test, strength increases with decreasing specimen size. However, the range in which this occurs is much smaller; at thicknesses of approximately two cell diameters, the bulk strength is reached.

To model the shear behavior, a regular hexagonal honeycomb was again used (see inset in Figure 2b). The cell walls were perfectly bonded to rigid plates at the top and bottom, resulting in clamped boundary conditions. For each integer value of T/d, the cell walls at the top and bottom plates were allowed to vary in length, ch and $(1 - c)h$, respectively, with $0 \le c \le 1$ and h being the length of the cell walls. Similar to the case of uniaxial compression, Euler–Bernoulli beam theory and limit-load analysis were used to obtain closed-form expressions for the shear stiffness and strength.[14] Here, only the shear strength is shown; similar conclusions hold for the stiffness.[14] For normalization,

$$\tau^*_{\text{bulk}} = \tfrac{1}{2}\sigma_{\text{ys}}(t/h)^2/\sqrt{3} \quad (2)$$

was used (σ_{ys} is the yield strength), which is valid for infinitely thick honeycombs.[15] Figure 2b shows that for $T/d = 1$, the stiffening effect is maximal for $c = 0.5$ and absent for $c = 0$. In a real foam, the length of cell walls at the boundary will be distributed randomly along the length of the specimen. To account for this in an average manner, an error bar was constructed in Figure 2b. Clearly, similar to the experimental results of Figure 2a, the strengthening effect is of short range, disappearing for specimens two cell diameters thick. A similar but more pronounced strengthening effect was obtained for randomized hexagons.[5] The underlying reason for the shear size effect is that the constrained rotations result in stiff and strong boundary layers at the top and bottom plates.

Indentation

Axisymmetric indentation tests were carried out on the closed-cell Alporas foam (see inset of Figure 3a). The indentation strength σ^*_{ind} was defined as the peak force (reached at an indenter displacement of approximately one-quarter of the cell size) divided by the indenter area. Figure 3a shows that the normalized indentation strength $\sigma^*_{\text{ind}}/\sigma^*_{\text{bulk}}$ increases when the normalized indenter size, D/d ($d = 4.5$ mm), decreases. The error bars (showing the standard deviation based on at least five different indentations) clearly indicate that the scatter also increases with decreasing indenter size.

A randomized hexagonal structure was used to model the indentation behavior, as shown in the inset of Figure 3b. A similar 2D model was used in References 5, 8, 16, and 17. A foam block 54 cells wide and 24 cells high was analyzed. The finite element method was used to discretize the cell structure into elastic/perfectly plastic Timoshenko beam elements (the material behaves elastically below the yield-stress value and "perfectly" plastically, i.e., without hardening, at the yield-stress value). These Timoshenko beam elements account for axial, shear, and bending deformation. The indenter was mimicked by applying vertical displacements while keeping the rotations constrained. Each data point in Figure 3b shows the average of five different random realizations, with the error bars representing the standard deviation. For each realization, the results are normalized by the specific value for the uniaxial-compression strength, approximately 1 MPa. Figure 3b clearly shows

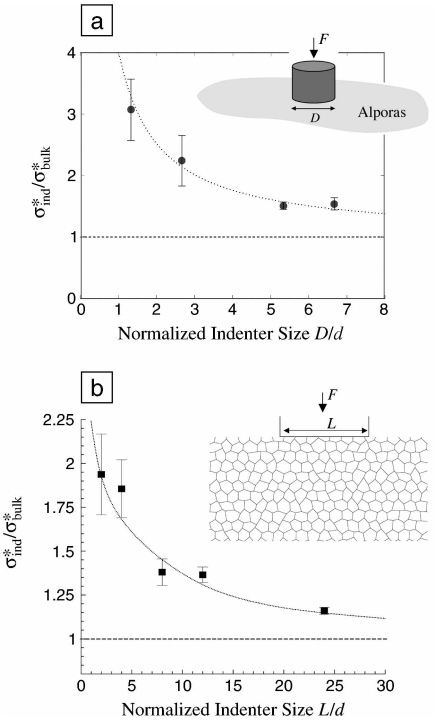

Figure 3. (a) Experimental indentation strength σ^*_{ind} normalized by the uniaxial compression strength σ^*_{bulk}, plotted against the indenter diameter D *normalized by the cell size* d *for the closed-cell Alporas foam (see inset). (b) Numerically obtained indentation strength σ^*_{ind} normalized by the uniaxial compression strength σ^*_{bulk}, plotted against the indenter length* L *normalized by the cell size* d *for a two-dimensional randomized hexagonal honeycomb (see inset).* F *indicates force.*

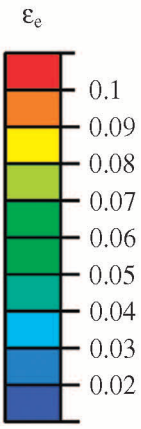

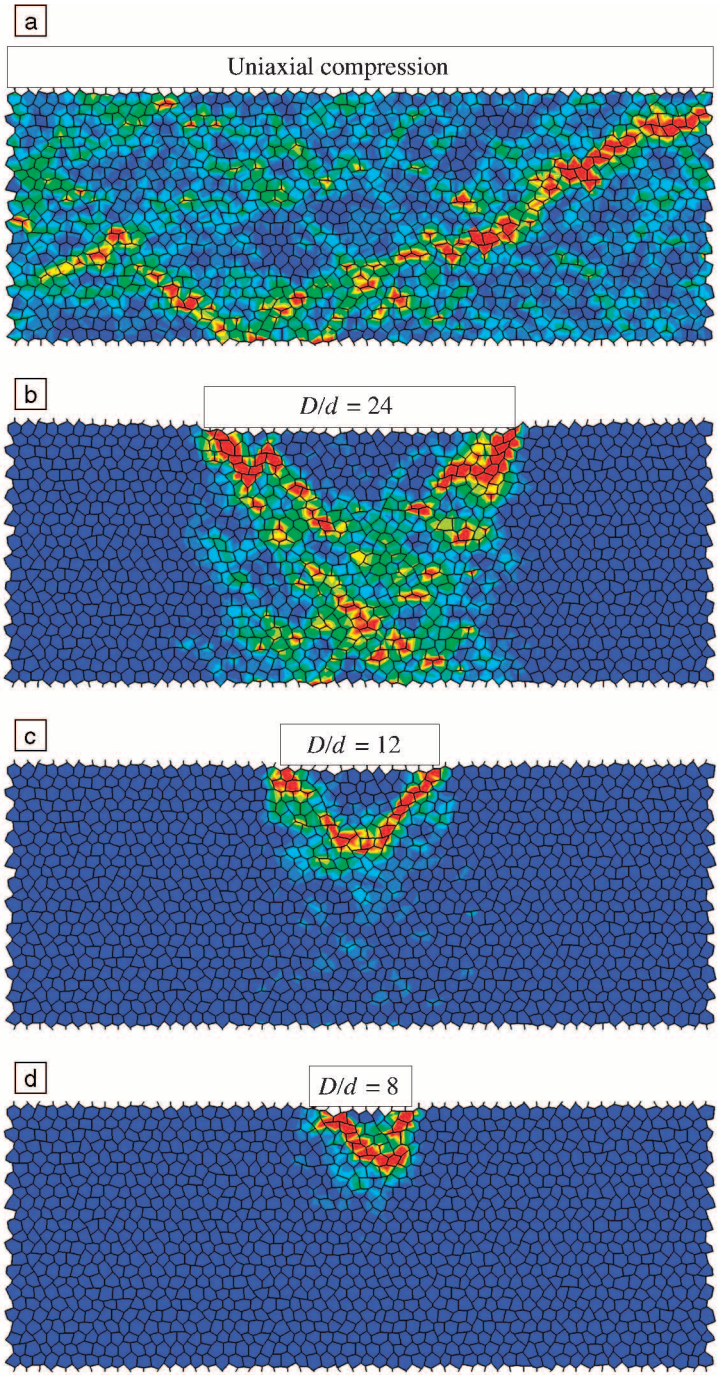

*Figure 4. Strain maps of indentation simulations, showing the accumulated effective cell strain ε_e on the deformed beam structure: (a) uniaxial compression, applied displacement = 0.69*d*; (b) normalized indenter size* D/d = *24, indenter displacement = 0.82*d*; (c)* D/d = *12, indenter displacement = 0.51*d*; (d)* D/d = *8, indenter displacement = 0.49*d.

that similar to the experimental results of Figure 3a, strength as well as scattering increases with decreasing indenter size. The results obtained here are in close agreement with previous results for a regular hexagonal honeycomb,[14] although the strengthening effect for the random structure is slightly larger.

To trace the origin of the size effect, the deformed microstructure was analyzed for different indenter sizes. Because the peak load is reached at relatively small applied displacements (one-quarter the cell size), the microstructural deformations were emphasized by using a strain mapping procedure, which computes for each cell the average strain from the cell's nodal displacements.[17] In Figure 4, the accumulated effective cell strain ε_e is plotted together with the deformed beam structure at an indenter displacement just after the peak load was reached. For uniaxial compression (Figure 4a), the strain localizes in a discrete band approximately one cell thick. This is in accordance with experimentally obtained strain maps.[4] For the indentation results, shear straining first concentrates at the indenter edges (Figure 4b), after which straining proceeds more in a crushing mode below the indenter, concentrating in discrete bands connecting the indenter edges (Figures 4c and 4d). As the indenter size decreases, the deformation becomes more localized.

Notch Effects

In order to study the compressive behavior of side-notched specimens, experiments[7,8] were performed on 8% dense closed-cell Alporas foam, with a cell size of approximately 3.5 mm. The DEN specimens were 60 mm wide, 100 mm high, and 40 mm thick (see upper inset in Figure 5). The net section strength σ^*_{net} was defined as the peak load from the force-displacement curve divided by the cross-sectional area $(W - a)t$, where W is the width of the sample, t is the thickness of the sample, and a is the combined depth of the notches. The individual experimental data points are plotted in Figure 5 (solid triangles), clearly showing that the normalized net section strength $\sigma^*_{net}/\sigma^*_{bulk}$ increases with increasing notch depth a/W. In other words, for deeper notches, more stress is needed to crush the material in the ligament area between the notches.

To model this notch-strengthening behavior, the same discrete microstructural model was used as in the section on indentation.[8,17] The specimen size was chosen to be 16 cells wide and 28 cells high, similar to the specimen dimensions used in the experiments. Calculations were performed on five different random realizations for each specimen geometry (see lower inset of Figure 5 for one specific realization for $a/W = 0.5$). In Figure 5, the average values (open squares) are plotted, accompanied by error bars to denote the standard deviation. Clearly, both the net section strength and the standard deviation increase with increasing notch depth. The numerical results are in close agreement with the experiments. Similar strengthening results were observed under tension, both experimentally[9–11] and numerically.[8,17,18] In Figure 6, the accumulated effective cell strain ε_e is plotted for $a/W = 0$, 0.25, 0.5, and 0.75 for the random realization shown in Figure 5 at a fixed overall displacement. Figure 6a ($a/W = 0$) corresponds to a uniaxial-compression test, showing the strain field at the moment the peak load is reached (similar to Figure 4a, but for a smaller applied displacement). When notches are introduced, shear strain first concentrates at the notch tips (Figure 6b), after which strain localizes in a discrete band spanning the ligament area between the notch tips. Strain becomes more localized as the notch depth increases (Figures 6c and 6d). These model strain maps are very similar to experimentally obtained strain maps, both in compression[8] and tension.[11,19] Clearly, the trend is very similar to the one observed in indentation (Figure 4), suggesting that the effect of the indenter size corresponds to the effect of the ligament area $(W - a)$. Compare Figure 4c with Figure 6b, for $D/d = 12$ and $(W - a)/d = 12$, and Figure 4d with Figure 6c, for $D/d = 8$ and $(W - a)/d = 8$.

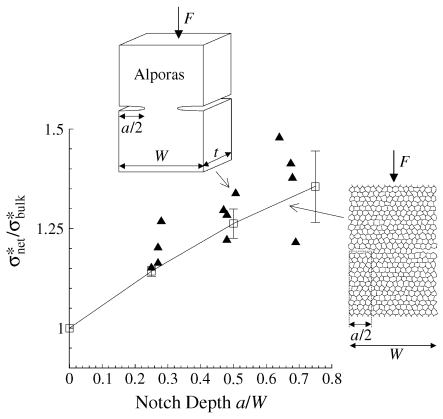

Figure 5. Net section strength σ^*_{net} normalized by the uniaxial-compression strength σ^*_{bulk}, plotted against notch depth a/W *for double-edge-notched specimens of 8% dense closed-cell Alporas foam with a cell size of approximately 3.5 mm (see insets). Specimens were 60 mm wide, 100 mm high, and 40 mm thick. The experimental data points are indicated by solid triangles and the numerical results by open squares.*

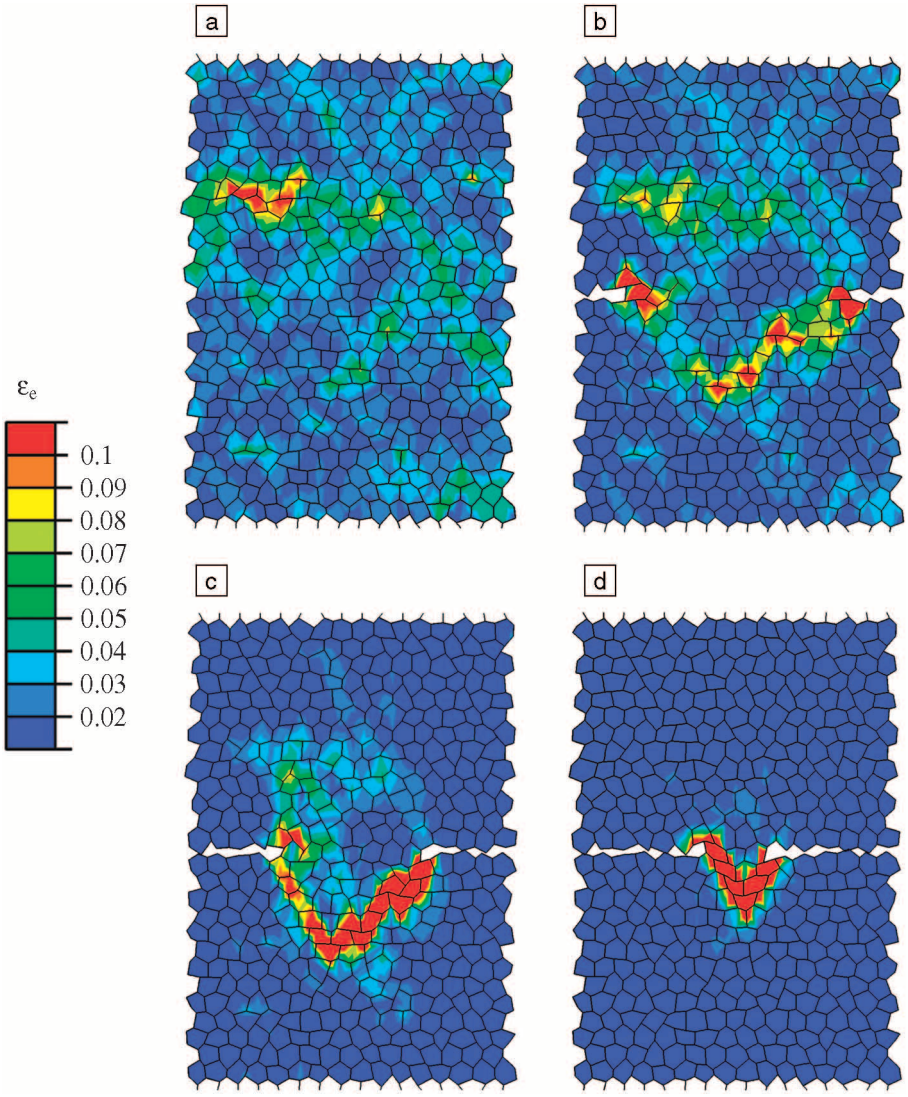

*Figure 6. Simulated strain maps of double-edge-notched specimens, showing the accumulated effective cell strain ε_e on the deformed beam structure at an applied displacement of 0.56*d*: (a) notch depth* a/W *= 0, (b)* a/W *= 0.25, (c)* a/W *= 0.5, (d)* a/W *= 0.75.*

Discussion

Scale effects in cellular metals occur when the specimen size is of the order of the cell size. This leads to material strengthening in shear, indentation, and in compression and tension of double-notched specimens when the relevant specimen dimensions are reduced. Alternatively, in uniaxial compression, reducing the specimen size leads to material weakening. Explanations for the scale effects can be classified in two categories: boundary-layer effects and constraint effects.

Boundary-layer effects are active under shear and uniaxial compression. In shear, the bonding of the specimen to rigid face sheets results in strong boundary layers, while in uniaxial compression, the free surface causes weak boundary layers. In both cases, the boundary layers are approximately one cell size thick.

Constraint effects are active in indentation and compression of DEN specimens. Bastawros et al.[4] showed that under uniaxial compression, the peak stress is reached at the moment plastic deformation localizes in discrete bands one cell thick. A key observation in their study is that this is not only related to randomly distributed irregularities that trigger the initiation of the bands, but to the ability of the surrounding material (above and below the deformation bands) to elastically accommodate the plastic deformation. In the case of indentation and compression of DEN specimens, the stress concentrations at the indenter edges and notch tips trigger early plastic shear deformation, as shown in Figures 4b and 6b. These strain concentrations set the end points between which the deformation pattern must develop. When the end points approach each other (with decreasing indenter size and increasing notch depth), the volume of material to be deformed decreases, reducing the number of irregularities available to trigger band formation. Moreover, the ability to elastically accommodate this band formation in such small volumes is severely constrained. The combination of these effects causes the strengthening behavior. This also explains why the strengthening is greater for indentation than for DEN specimens (see Figures 3 and 5), because the volume of material below the indenter to be deformed is half of that between the notch tips (compare, for example, Figures 4c and 6b). Also, the increased scatter with decreasing indenter size (Figure 3) and cross-sectional area (Figure 5) can be explained by referring to the stochastics of finding a unique deformation path in a decreasing volume of material.

Recent numerical calculations with the same discrete model used here showed that single-edge-notched (SEN) specimens and center-cracked panels (CCPs) under compression are notch-insensitive,[8] as was also observed experimentally.[13] The reason for this is that the specific DEN constraint (imposing the deformation pattern to connect the strain concentrations at the notch tips) is completely absent in SEN specimens and CCPs, leaving the material in the ligament as unconstrained as in a uniaxial-compression test.

Care should be taken in extrapolating the modeling results to real 3D foams. Based on dimensional arguments, the 2D modeling results for uniaxial compression and indentation cannot be directly extended to three dimensions because of the specific 3D geometry of the test configurations. In contrast, the results for shear and DEN specimens can be used as an approximation for 3D foams, because the specimens are taken to be thick enough that no strain gradients develop in the out-of-plane direction.

Acknowledgments

The author acknowledges close collaborations with John Hutchinson, Lorna Gibson, Erik Andrews, and Ashraf Bastawros, on which this paper has been based. Onck's research was made possible by a fellowship from the Royal Netherlands Academy of Arts and Sciences.

References

1. M.F. Ashby, A.G. Evans, N.A. Fleck, L.J. Gibson, L.W. Hutchinson, and H.G. Wadley, *Metal Foams: A Design Guide* (Butterworth-Heinemann, Oxford, UK, 2000).
2. A.G. Evans, J.W. Hutchinson, and M.F. Ashby, *Prog. Mater. Sci.* **43** (1998) p. 171.
3. E.W. Andrews, G. Gioux, P.R. Onck, and L.J. Gibson, *Int. J. Mech. Sci.* **34** (2000) p. 701.
4. A.-F. Bastawros, H. Bart-Smith, and A.G. Evans, *J. Mech. Phys. Solids* **48** (2000) p. 301.
5. C. Chen and N.A. Fleck, *J. Mech. Phys. Solids* **50** (2002) p. 955.
6. O.B. Olurin, N.A. Fleck, and M.F. Ashby, *Scripta Mater.* **43** (2000) p. 983.
7. P.R. Onck and A.-F. Bastawros, in *Advances in Mechanical Behaviour, Plasticity and Damage,* edited by D. Miannay, P. Costa, D. Francois, and A. Pineau (Elsevier, Amsterdam, 2000) p. 717.
8. P.R. Onck, A.A. Maki, and A.-F. Bastawros (unpublished manuscript).
9. O.B. Olurin, N.A. Fleck, and M.F. Ashby, *Mater. Sci. Eng., A* **291** (2000) p. 136.
10. E.W. Andrews and L.J. Gibson, *Scripta Mater.* **44** (2001) p. 1005.
11. C. Motz and R. Pippan, *Acta Mater.* **49** (2001) p. 2463.
12. Y. Sugimura, J. Meyer, M.Y. He, H. Bart-Smith, J. Grenestedt, and A.G. Evans, *Acta Mater.* **45** (1997) p. 5245.
13. A. Paul, T. Seshacharyulu, and U. Ramamurty, *Scripta Mater.* **40** (1999) p. 809.
14. P.R. Onck, E.W. Andrews, and L.J. Gibson, *Int. J. Mech. Sci.* **34** (2000) p. 681.
15. L.J. Gibson and M.F. Ashby, *Cellular Solids: Structure and Properties,* 2nd ed. (Cambridge University Press, Cambridge, 1997).
16. C. Chen, T.J. Lu, and N.A. Fleck, *J. Mech. Phys. Solids* **47** (1999) p. 2235.
17. P.R. Onck, *J. Phys. IV* **11** (2001) p. 211.
18. E.W. Andrews and L.J. Gibson, *Acta Mater.* **49** (2001) p. 2975.
19. E.W. Andrews and L.J. Gibson, *Mater. Lett.* **57** (3) (2002) p. 53. □